Supplementary Information for

Direct photoconversion of CO_2 to carbon nanotubes for oxygen recycling in extraterrestrial exploration

Jun Wang[a,b,1], Jiajia Wang[c,1], Jianyong Feng[a,b,2], Yingfei Hu[a], Huiting Huang[b], Ningsi Zhang[b], Minyue Zhao[b], Changhao Liu[b], Zhi Zhu[a], Shicheng Yan[b,2], Tao Yu[a], Ce Zhang[d], Wei Yao[d], Zhaosheng Li[a,b,2], Zhigang Zou[a,b]

[a]Collaborative Innovation Center of Advanced Microstructures, National Laboratory of Solid State Microstructures, School of Physics, Nanjing University, Nanjing, 210093, P.R. China
[b]Jiangsu Key Laboratory for Nano Technology, College of Engineering and Applied Sciences, Nanjing University, Nanjing, 210093, P.R. China
[c]College of Mechanics and Materials, Hohai University, Nanjing 210098, P.R. China
[d]Qian Xuesen Laboratory of Space Technology, China Academy of Space Technology, Beijing 100094, P.R. China

[1]J.W. and J.J.W. contributed equally to this work.
[2]To whom correspondence may be addressed. E-mail: fengjianyong@nju.edu.cn; yscfei@nju.edu.cn; zsli@nju.edu.cn.

This PDF file includes:

Supplementary Information Text

Experimental Procedures

Materials

Commercially available Co_3O_4 (CP, Sinopharm Chemical Reagent Co., Ltd.), CoO (CP, Sinopharm Chemical Reagent Co., Ltd.) and cobalt powder (99.5%, Shanghai Aladdin Biochemical Technology Co., Ltd.) were used as received without further purification.

Sample characterization

For phase identification of the samples, X-ray diffraction (XRD) patterns were collected on an X-ray diffractometer (Ultima III, Rigaku) with Cu Kα radiation working at 40 kV, 40 mA. The morphologies of the samples were observed by a field-emission scanning electron microscopy (FESEM, Gemini 500, Zeiss). The transmission electron microscope (TEM, Tecnai G2 F30, FEI) equipped with an energy dispersive X-ray spectroscopy (EDX) was used to obtain more morphological and compositional information of the samples, which operated at an accelerating voltage of 200 kV. High-angle annular dark-field (HAADF) scanning transmission electron microscopy (STEM) images were obtained by a JEOL JEM-ARM200F microscope incorporated with a spherical aberration correction system for STEM. Surface analysis of the samples was carried out on an X-ray photoelectron spectrometer (XPS, K-Alpha+, Thermo Scientific) with binding energy calibrated to C 1s peak at 284.8 eV. Raman spectra of the samples were collected by using a WITec Raman imaging system (Alpha 300R) and a confocal laser Raman spectrometer (LabRAM Aramis, Horiba, calibrated with silicon) with excitation wavelength of 488 nm and 532 nm, respectively. The H_2-temperature programmed reduction (H_2-TPR) and the CO_2-temperature programmed desorption (CO_2-TPD) measurements were carried out on a chemisorption analyzer (AutoChem II 2920, Micromeritics).

X-ray absorption fine structure spectroscopy measurements

The X-ray absorption fine structure spectra were collected with Si (111) crystal monochromators at the BL11B beamlines in Shanghai Synchrotron Radiation Facility (SSRF) (Shanghai, China). Before measured at the beamline, samples were pressed into pellets with 1 cm in diameter and sealed using Kapton tapes. Co K-edge extended X-ray absorption fine structure (EXAFS) spectra and XAFS spectra of the standard samples (Co foil, CoO, and Co_3O_4) were recorded in a transmission mode at room temperature using a 4-channel silicon drift detector (SDD, Bruker 5040). Negligible changes in the line-shape and peak position of Co K-edge XANES spectra were observed between two scans taken for a specific sample. The spectra were processed

and analyzed by the analysis programs, Athena and Artemis. Settings for curvefit parameters are shown in Table S1.

Catalyst testing procedure and product analysis

Catalytic hydrogenation of CO_2 over the cobalt-bearing catalyst was conducted in a gas-tight system with a 300 W Xenon lamp (Beijing CEAuLight Technology Co., Ltd or Shenyang Yirda Technology Co., Ltd) as the light source. In a typical test, 30 mg of the catalyst was dispersed on a quartz microfiber filter of 3.2 cm in diameter (Whatman, QMA 1851-032), and then placed in a 420 mL reactor cell equipped with a quartz window on the top. Certain amounts of CO_2 and H_2 were introduced sequentially into the testing system after evacuation, then the reaction system was kept sealed. Prior to irradiation, the feed gas was mixed thoroughly with the help of a gas circulator under the system pressure of ~0.07 MPa. The gas sample was collected by a gas tight syringe and then analyzed on a gas chromatograph (GC9790PLUS, Zhejiang Fuli Analytical Instrument Co., Ltd) using a thermal conductivity detector (TCD) after the catalyst test was completed. In the isotopic labeling experiment, ^{13}C-carbon dioxide ($^{13}CO_2$) and hydrogen were used as the mixed feed gas instead. The pyrolysis behavior of the formed solid product and the released gas were then analyzed by a thermogravimetric analyzer equipped with mass spectrometry (TGA-MS, Thermo plus EV/Thermo Mass Photo, Rigaku) under flowing air.

Thermocatalytic test was also carried out as a control experiment. Briefly, 30 mg of the catalyst was dispersed on a quartz microfiber filter of 3.2 cm in diameter (Whatman, QMA 1851-032), and then placed in a quartz tube (inner diameter 4.5 cm, length 150 cm) equipped with sealing flanges. The feed gas (the molar ratio of CO_2 to H_2 is 1:2) runs through the quartz tube for hours to exhaust air. After that, the quartz tube was sealed and heated at 400 °C for 10 hours.

H_2-temperature programmed reduction (H_2-TPR) experiment

H_2-TPR experiment was carried out in a quartz tube fixed-bed micro-reactor. The sample (100 mg) was treated in flowing He at ambient temperature for 1 h, and then heated from ambient temperature to 800 °C (10 ℃/min) in a flow of 10% H_2/Ar (30 mL/min). The H_2 consumption was recorded by a TCD.

CO_2-temperature programmed desorption (CO_2-TPD) experiments

For pristine Co_3O_4 catalyst, CO_2-TPD experiment was carried out in a quartz tube fixed-bed micro-reactor. Prior to the analyses, the sample (100 mg) was treated in flowing He (30 mL/min) at 300 °C for 1 h to remove the residual adsorbed water, and exposured to CO_2/Ar (30 mL/min) for an additional hour at room temperature. Afterwards, it was

purged with He (30 mL/min) at the same temperature until the baseline of the CO_2 signal leveled off. Temperature CO_2 desorption was followed by recording the TCD signal up to 600 °C (10 °C /min).

For H_2-treated Co_3O_4 catalyst, CO_2-TPD experiment was carried out in the same quartz tube fixed-bed micro-reactor. Before the TPD experiment, Co_3O_4 (100 mg) was treated in flowing He (30 mL/min) at 300 °C for 1 h to remove the residual adsorbed water. The H_2-treated Co_3O_4 catalyst was formed by heating Co_3O_4 from room temperature to 400 °C (10 °C /min) and maintained at 400 °C for 2 h in a flow of 10% H_2/Ar (30 mL/min), during which the H_2 consumption was recorded by a TCD. After the formation of H_2-reduced Co_3O_4, the sample was cooled down to room temperature and then purged with He (30 mL/min) at ambient temperature for 1 h. Prior to the analyses, the catalyst was exposed to CO_2/Ar (30 mL/min) for 1 h at room temperature, then purged with He (30 mL/min) at the same temperature until the baseline of the CO_2 signal leveled off. Then it was heated (10 °C /min) from room temperature up to 600 °C. Temperature CO_2 desorption throughout the heating process was monitored by means of a TCD.

In-situ diffuse reflectance infrared Fourier transform spectroscopy (DRIFTS) experiments

The in-situ DRIFTS measurements were performed on a Fourier-transform infrared spectrometer (iS50, Nicolet, Thermo Scientific) equipped with an MCT detector. Before the measurement, Co_3O_4 (150 mg) was treated in flowing Ar (50 mL/min) at 400 °C for 1 h to remove the residual adsorbed water. The background spectra were collected at different temperatures. Then the catalyst was exposed to a mixture of CO_2 (33 %) and H_2 (66 %) (30 mL/min) (or a mixture of CO (50 %) and H_2 (50 %)) for 10 min. Afterwards, the reaction chamber was sealed, and the in-situ DRIFT spectra in dark and under light illumination were recorded at different times and temperatures by recording 32 scans at 4 cm^{-1} resolution.

Electrochemical Measurements

The three-electrode system was used to carry out electrochemical measurements by a CHI 660E (CH Instrument) electrochemical workstation. The rotating disk electrode (RDE, 0.196 cm^{-2}) with coated catalyst was employed as the working electrode, the counter electrode was a graphite rod, and the reference electrode was a Hg/HgO electrode. The electrolyte was 1.0 M NaOH aqueous solution. The coating slurry was prepared by ultrasonication of the mixture of catalysts (10 mg) after the catalytic testing, 325 μL ethanol, and 95 μL Nafion (5 wt. %) for 20 min. Then the working electrode was prepared by dropping the slurry (7 μL) onto the glassy carbon surface of RDE.

According to the Nernst equation, $E_{RHE} = E_{ref} + 0.059 \times pH + E_{measured}$, the applied potential with respect to the reversible hydrogen electrode (RHE) can be obtained from the measured electrode potential. The linear sweep voltammetry (LSV) was determined at the scan rate of 30 mV s^{-1} under 1600 rpm. The chronopotentiometric curves were obtained at a current density of 10 mA cm^{-2}.

Calculation of Raman band frequencies of ^{13}C CNTs

According to the harmonic oscillator model in classical mechanics, the square of vibration frequency is inversely proportional to the mass of oscillator.

$$\omega^2 = k / m$$

where k is spring constant.

Hence, the band frequencies of ^{13}C CNT can be estimate on the basis of the following equation,

$$\omega_{13} = \omega_{12} (m_{12} / m_{13})^{1/2}$$

where ω_{12} is the characteristic band frequencies of ^{12}C CNT. The calculated D, G and 2D band frequencies of ^{13}C CNT are 1293, 1525 and 2592 cm^{-1} respectively, which are accorded well with the experimental value in Fig. 2b.

Calculation of turnover number (TON)

Turnover number (TON) of Co-based catalyst towards CNT formation is determined by the following equation:

$$TON = n(C) / n(Co)$$

where n(C) is the molar quantity of carbon in produced CNTs (the quantity of CNTs is based on TGA results), and n(Co) is the mole quantity of Co used in the test.

As shown in Fig. S16, the turnover numbers after 10 h and 30 h are approximately 1.6 and 2.8, respectively, indicating that the photochemical CNT formation process is a catalytic reaction. To further certify that the photochemical CNT formation process is a catalytic reaction, we carried out a four-run photochemical reaction (10 h/run) in a pressure vessel. In every run, a flow of CO_2 and H_2 were introduced sequentially into the testing system after evacuation.

After the four-run (10 h/run) photochemical reaction at 1MPa, the calculated TON of the Co-based catalyst can reach 160, confirming that the photochemical CNT formation process on the Co-based catalyst is a catalytic reaction.

Calculation of CNT content

The amount of CNTs based on carbon is determined by the following equations:

$$m(C) = m(Co_3O_4) * loss / (100\%–loss)$$

$$n(C) = m(C) / M(C)$$

$$\text{CNT percentage} = n(C) / n(CO_2) * 100\%$$

where m(C) is the mass of carbon, $m(Co_3O_4)$ is the mass of catalyst, loss is the weight loss of the particles (solid products and the catalyst) measured by a thermogravimetric analyzer, n(C) is the molar quantity of carbon in produced CNTs, M(C) is the molar mass of carbon (12 g mol^{-1}), $n(CO_2)$ is the initial amount of CO_2 (~4 mmol).

Computational methods

The density functional theory (DFT) calculations are performed using VASP[1] with a projected augmented wave (PAW[2]) method. The generalized gradient approximation (GGA[3]) in the scheme of Perdew–Burke–Ernzerhof (PBE[4]) is selected as the exchange correlation functional. The cutoff energy is 500 eV. Geometry relaxations are performed until the residual forces on each ion converge to be smaller than 0.04 eV $Å^{-1}$. For C, O and Co elements, the $2s^22p^2$, $2s^22p^6$ and $3d^84s^1$ orbitals, respectively, are treated as valence states. To calculate free energy of reaction, the free energy of every term in the reaction should be calculated. The free energies of slab models are calculated by standard thermodynamic methods[5]:

$$G^{slab} = E^{DFT} + E^{ZPC} + E^{V} - TS^{V}$$

where E^{DFT} refers to the electronic energy directly calculated form DFT calculations, E^{ZPC} is zero-point energy correction, E^{v} and S^{v} are vibrational contributions to the internal energy and the entropy, respectively, and T is temperature.

Thanks to the VASPKIT[6], which is a powerful post-processing program for VASP, all the energy terms in the above equation can be easily calculated and the final free energy can be obtained. The calculated free energies of different slab models are listed in Table S2.

The conventional cells of hcp-Co and fcc-Co are firstly relaxed. The relaxed lattice constants of hcp-Co and fcc-Co are (a=b=2.51 Å, c=4.07 Å) and (a=b=c=3.54 Å), respectively, which are in good agreement with experiments. Then, the surface models can be constructed from the relaxed conventional cells. For hcp-Co, we select the typical close packed (001) plane of hexagonal crystal to build slab model. For fcc-Co, its (100) surface was reported to be more active to adsorbates[7], we therefore selected fcc-Co (100) surface to build slab model. Fig. S24a and b show the super-cell slab models of 4×4 hcp-Co (001) and 2×2 fcc-Co (100) surfaces, respectively. Due to the large size of super-cells, the Brillouin zone is sampled only by the Gamma *k*-point. For each slab model, a vacuum space of 12 Å is added to avoid interaction between mirror images. Every slab model contains five atomic layers, which have been proven to be sufficient to simultaneously simulate the surface and bulk regions[7,8]. During geometry relaxation, the bottom two atomic layers are fixed while other atomic layers, as well as

the adsorbates, are allowed to move. When different adsorbates are adsorbed on the slab models, possible initial structures are considered. For example, on the fcc-Co (100) surface, the CO adsorbate may interact with surface cobalt atom through O atom (Fig. S24c) or C atom (Fig. S24d). Then, the most stable adsorption model will be finally selected.

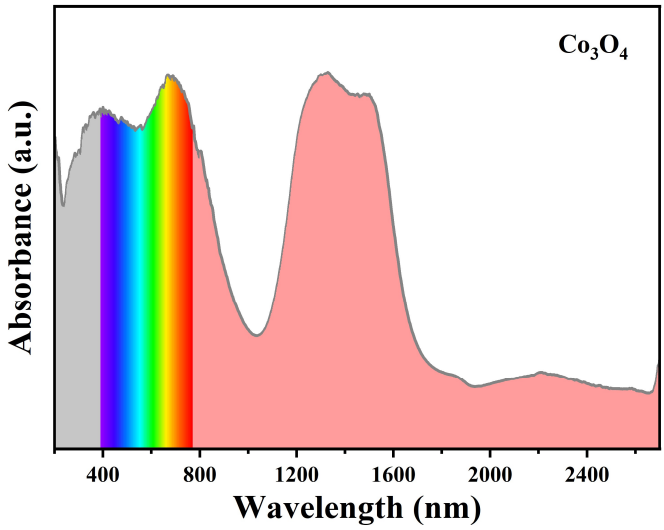

214

215 **Fig. S1.** Absorption spectrum of Co_3O_4.

216

217

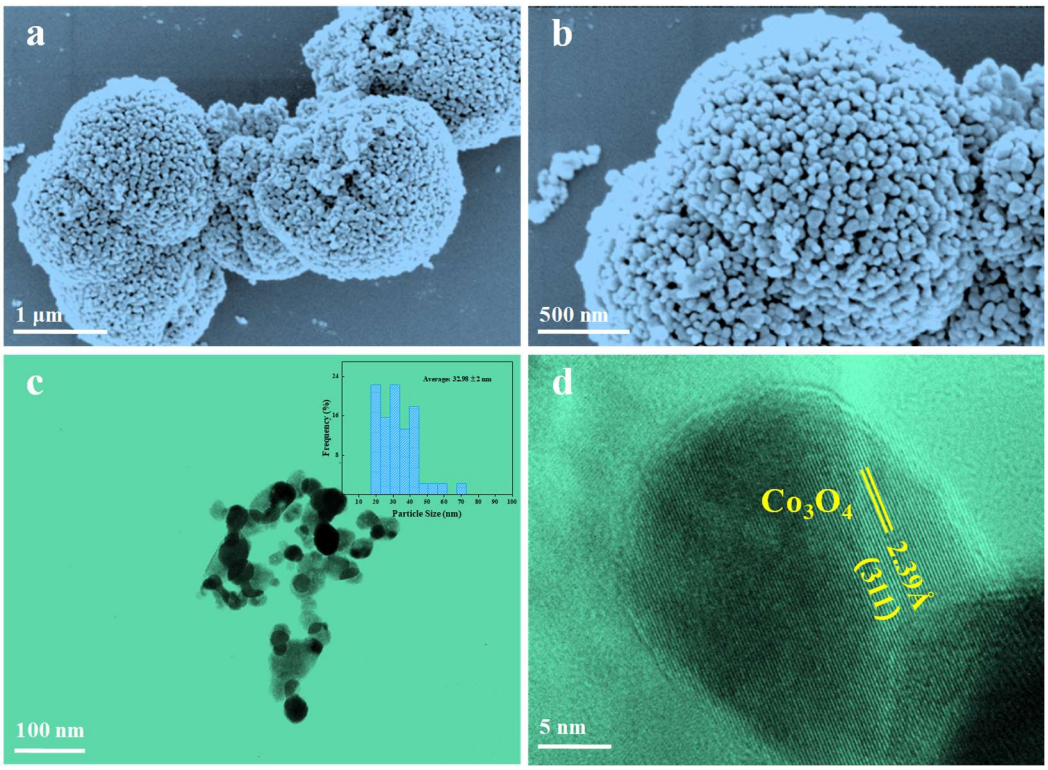

Fig. S2. SEM (**a**,**b**) and TEM (**c**,**d**) images of Co_3O_4 catalyst.

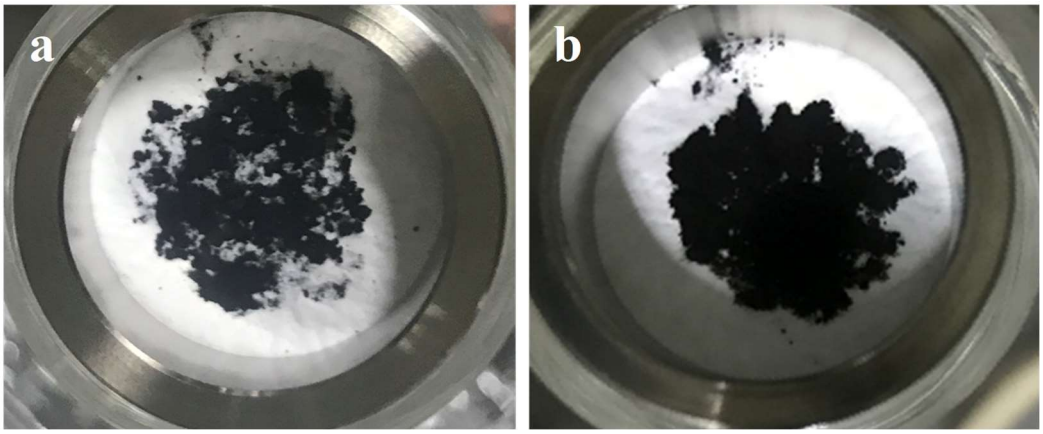

Fig. S3. Photographs of Co_3O_4 catalyst before (**a**) and after (**b**) a 5-h photochemical reaction.

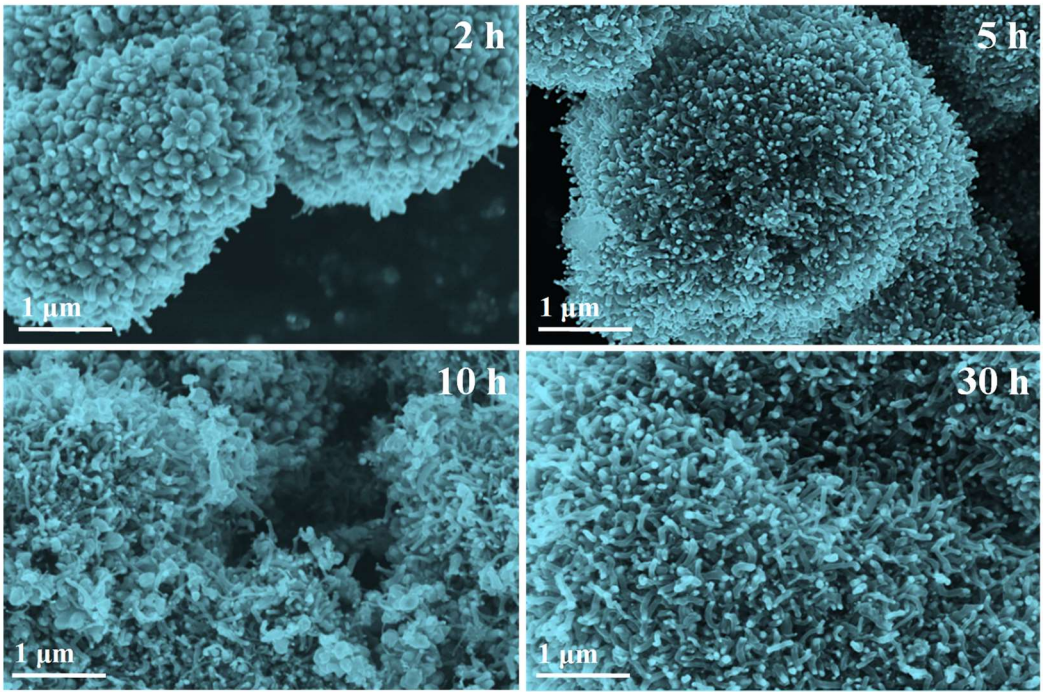

227

228 **Fig. S4.** SEM images of catalyst after different photochemical reaction times.

229

230

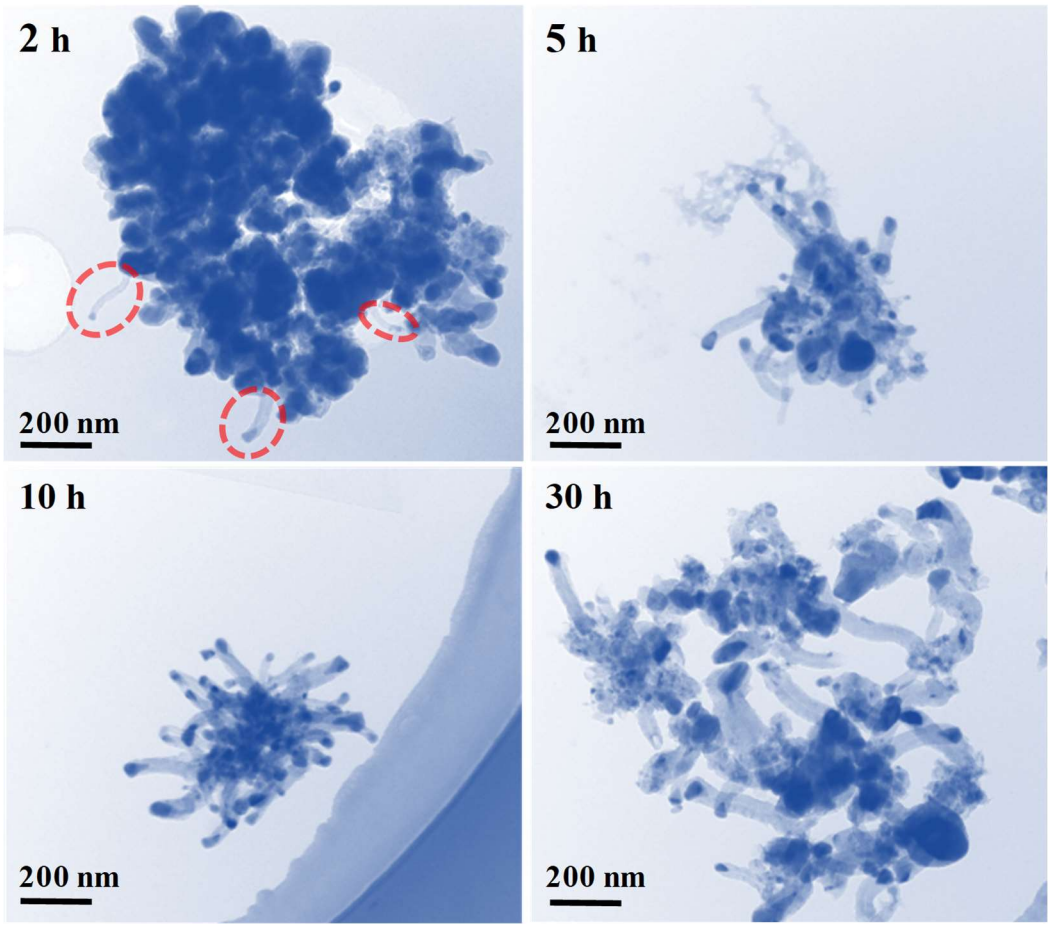

231

232 **Fig. S5.** TEM images of catalyst after different photochemical reaction times.

233

234

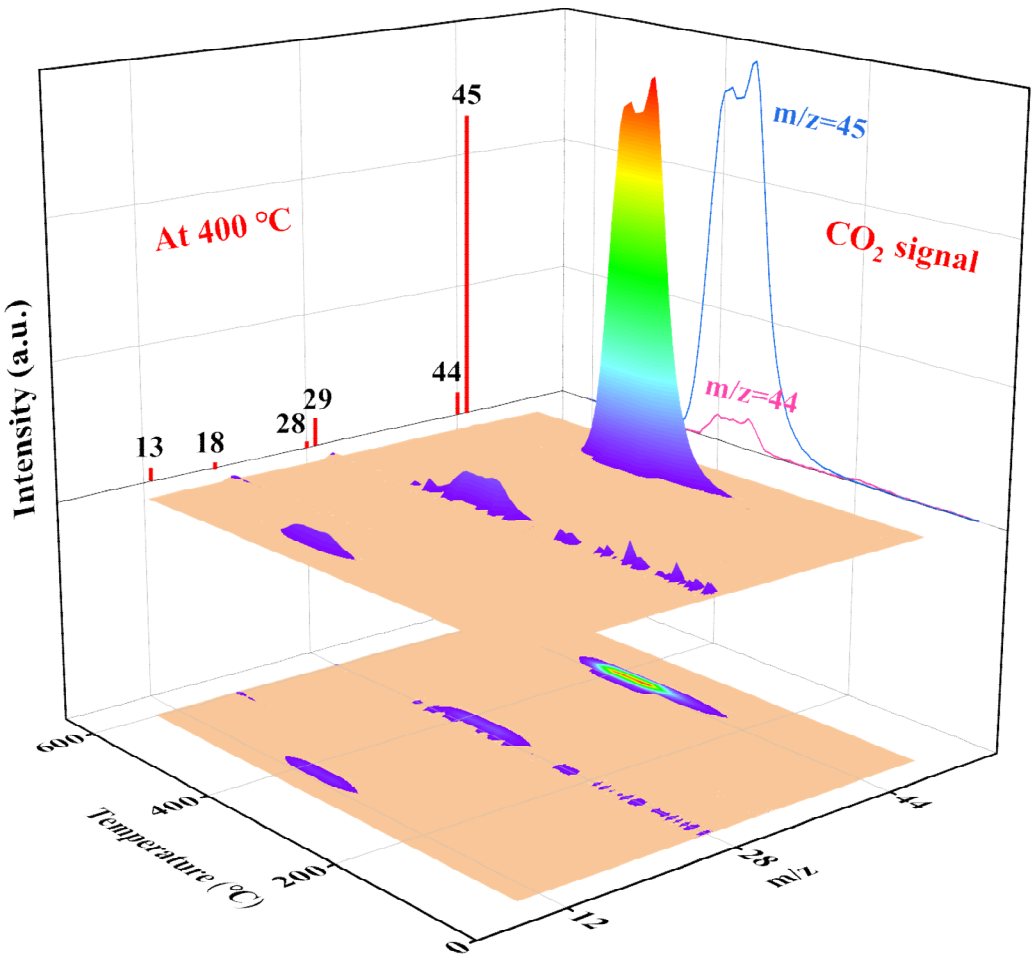

235

236 **Fig. S6.** Detailed real-time mass spectra of Fig. 1c.

237

238

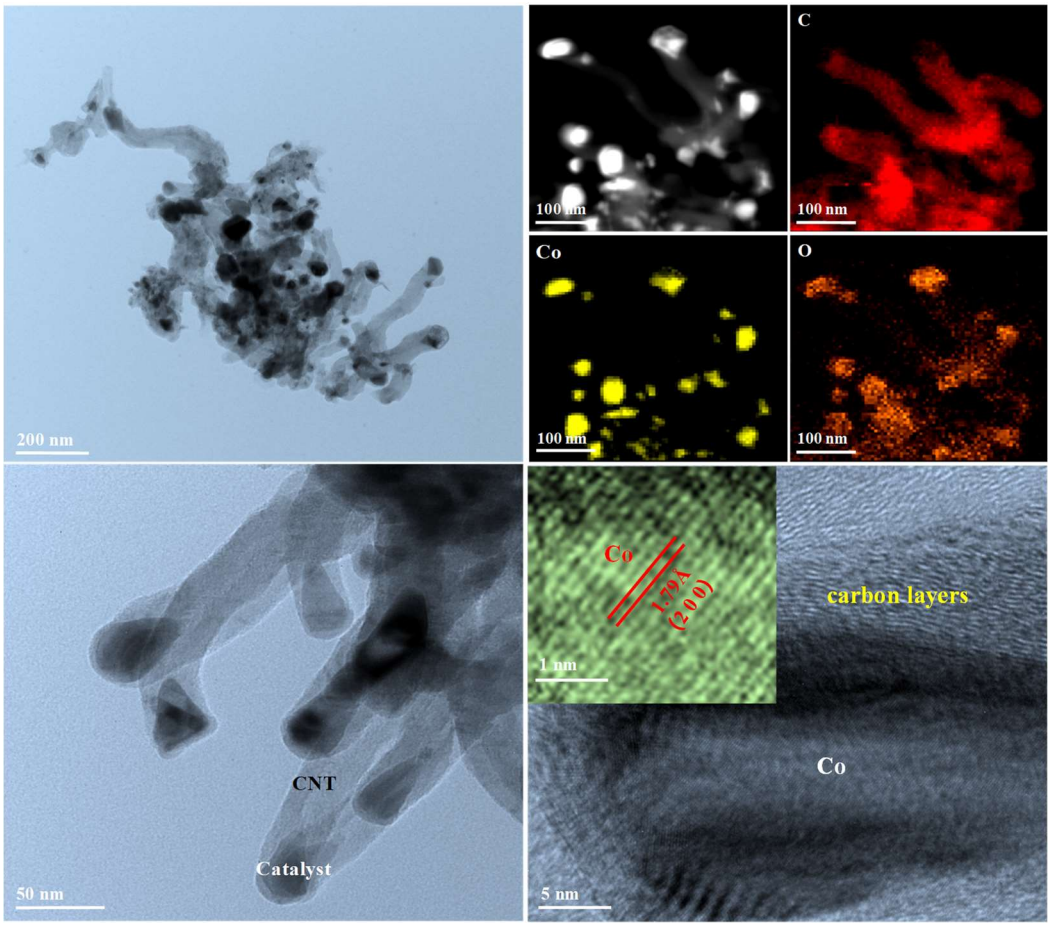

Fig. S7. TEM, HRTEM images and EDX elemental mapping of the catalyst after a 5-h photochemical reaction.

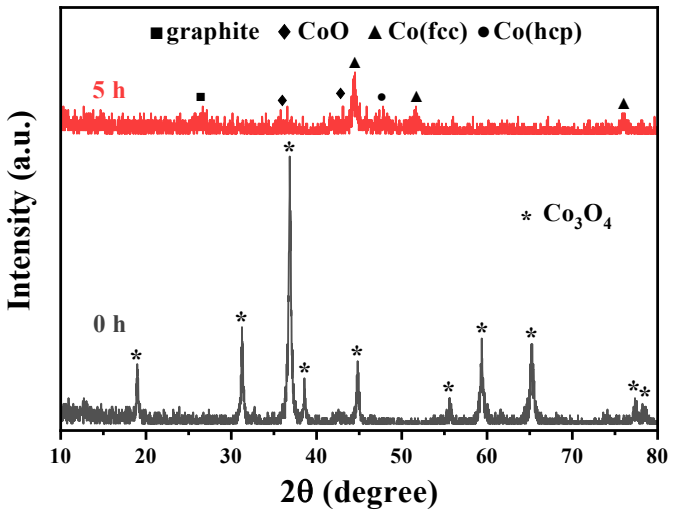

245

246 **Fig. S8.** XRD patterns of the catalyst before and after a 5-h photochemical reaction.

247

248

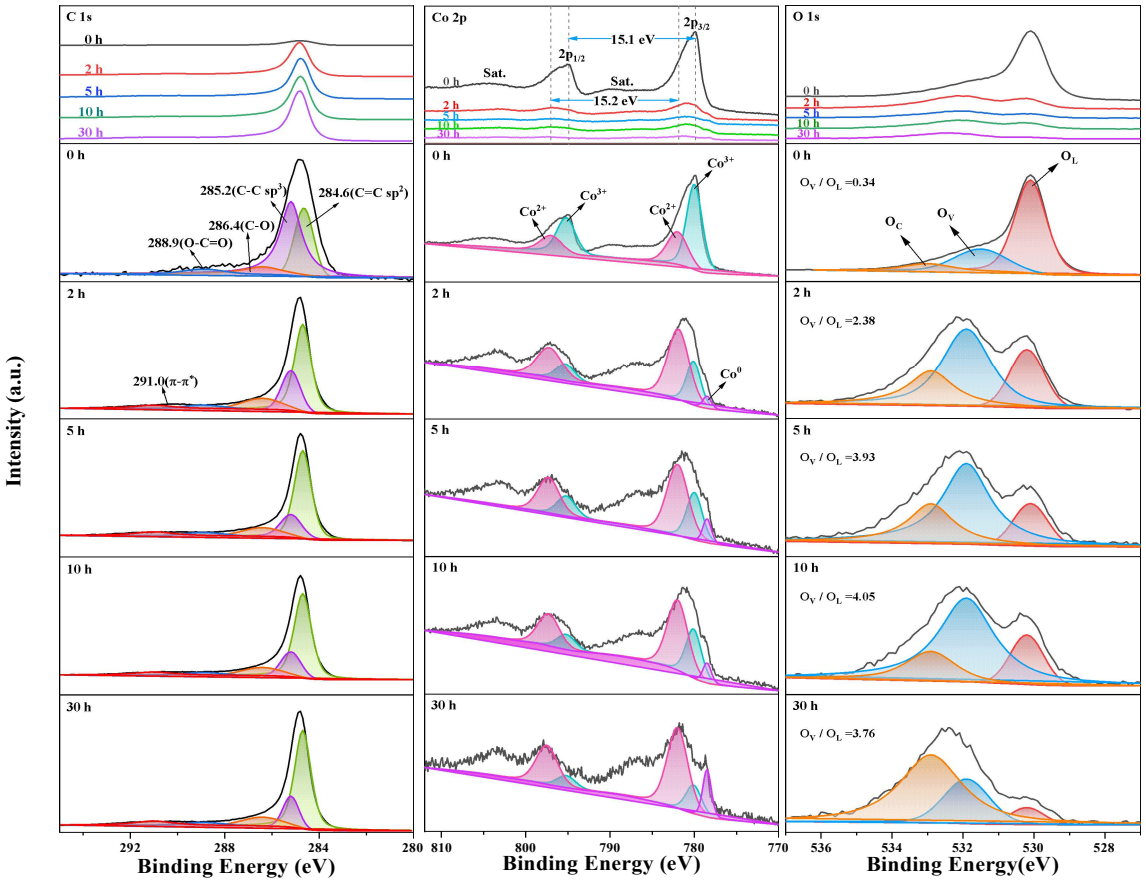

Fig. S9. C 1s, Co 2p and O 2p XPS spectra of the catalyst before and after the photochemical reaction. O_L, lattice O^{2-}; O_V, oxygen vacancy; O_C, adsorbed water or hydroxyl groups.

255 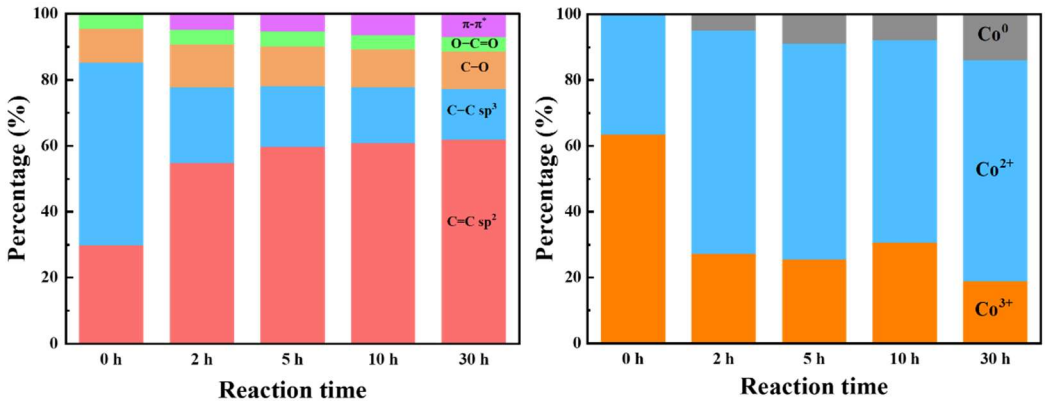

256 **Fig. S10.** Evolution of different carbon and cobalt species in catalyst along with
257 photochemical reaction time based on XPS spectra.

258

259

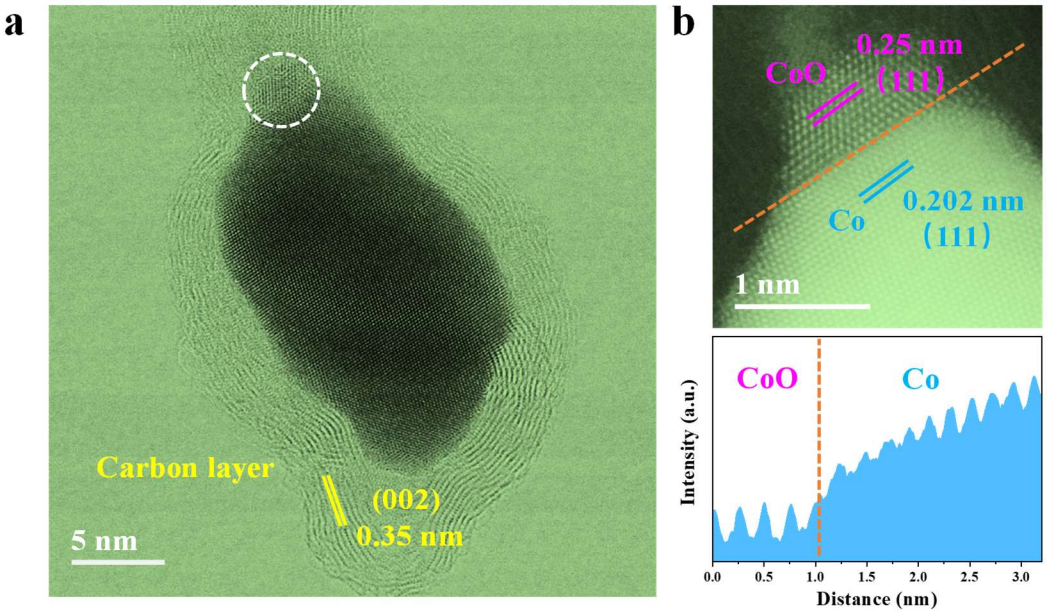

260

261 **Fig. S11. a**, Enlarged image of Fig. 2a. **b**, HRTEM image of the selected area by a white
262 circle in **a**, and the corresponding pixel intensity profiles at the interface of CoO and
263 Co phases.

264

265

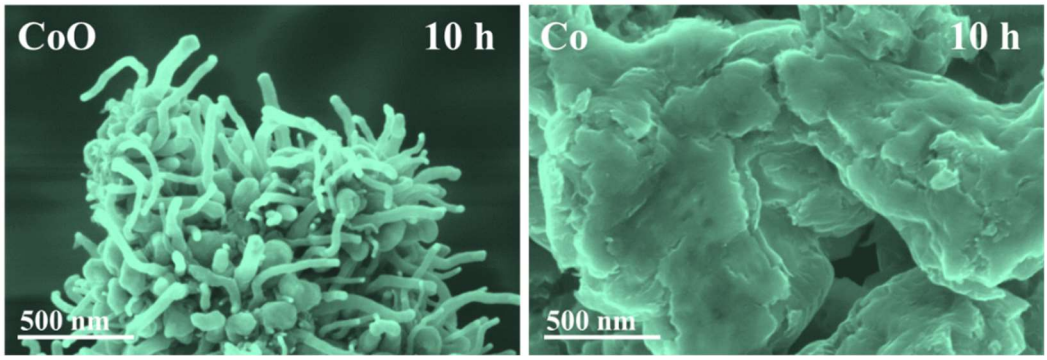

Fig. S12. SEM images of CoO and Co after a 10-h photochemical reaction.

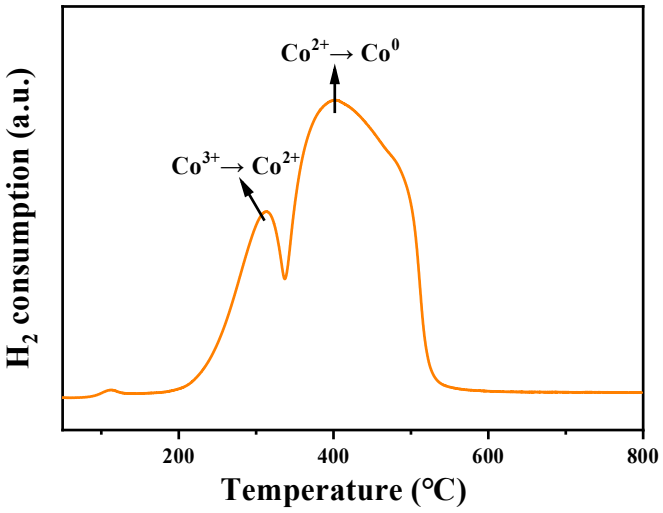

Fig. S13. H_2-TPR profile of Co_3O_4 catalyst in a flow of 10% H_2/Ar (30 mL/min) at a ramping rate of 10 °C/min.

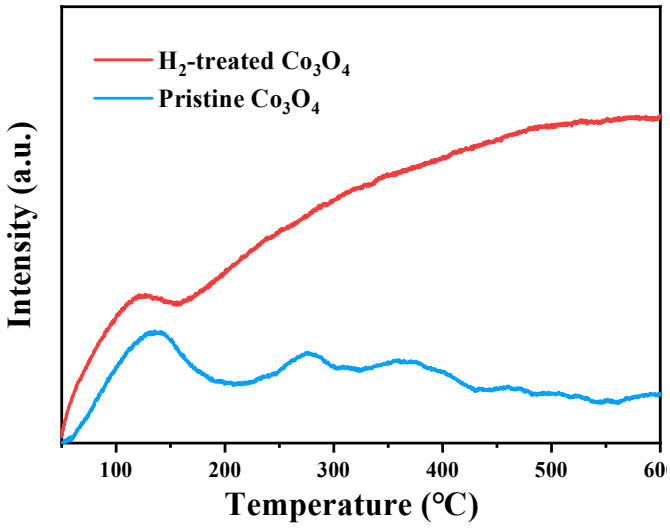

275

276 **Fig. S14.** CO_2-TPD profiles of Co_3O_4 catalyst with and without H_2 treatment at a
277 ramping rate of 10 °C/min.

278

279

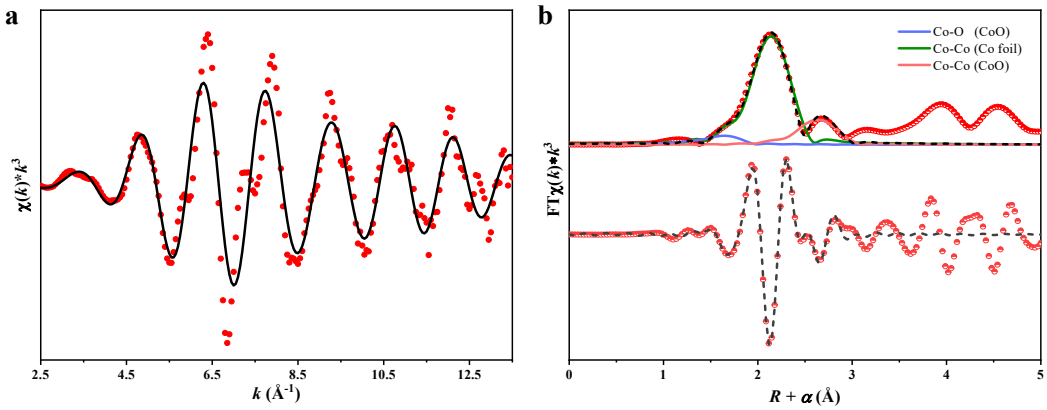

280

281 **Fig. S15. a**, Co K-edge EXAFS (red spots) and the fitted curve (black line) for the CoO_x
282 catalyst, shown in k^3-weighted k-space. **b**, Co K-edge EXAFS (red spots) and fitted
283 curves (dashed lines) for the CoO_x catalyst, shown in R-space (FT magnitude and
284 imaginary component). The data is k^3-weighted and not phase-corrected.

285

286

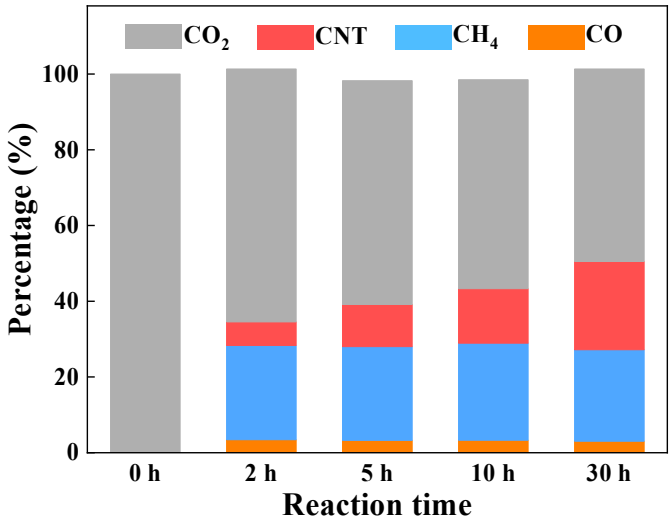

287

288 **Fig. S16.** Molar percentages (based on C) of CO_2, CNT, CH_4 and CO after different
289 photochemical reaction times.

290

291

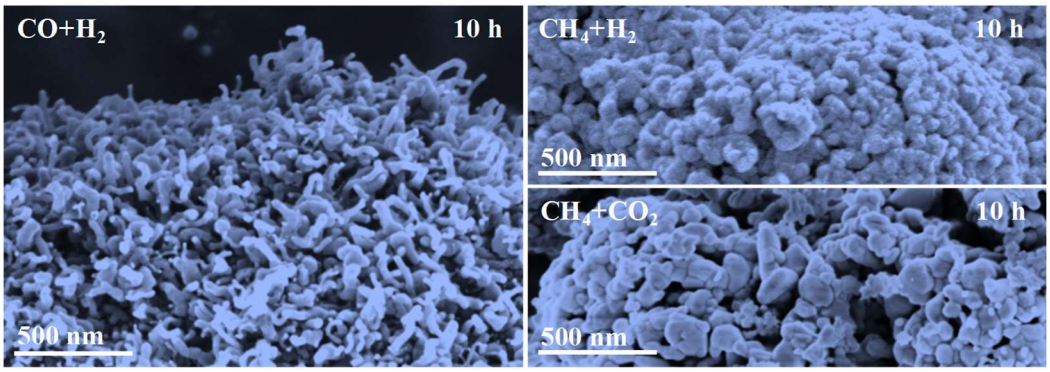

Fig. S17. SEM images of Co_3O_4 after a 10-h photochemical reaction using different feed gases.

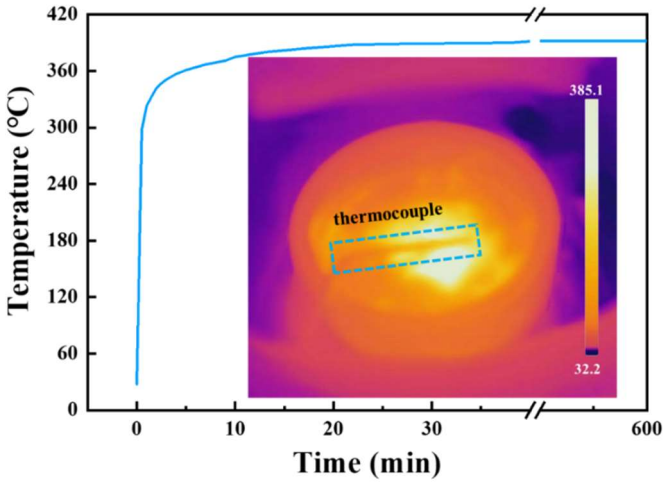

297

298 **Fig. S18.** Temperature evolution and spatial temperature mapping of the catalyst upon
299 Xe-lamp irradiation (4 W·cm^{-2}).

300

301

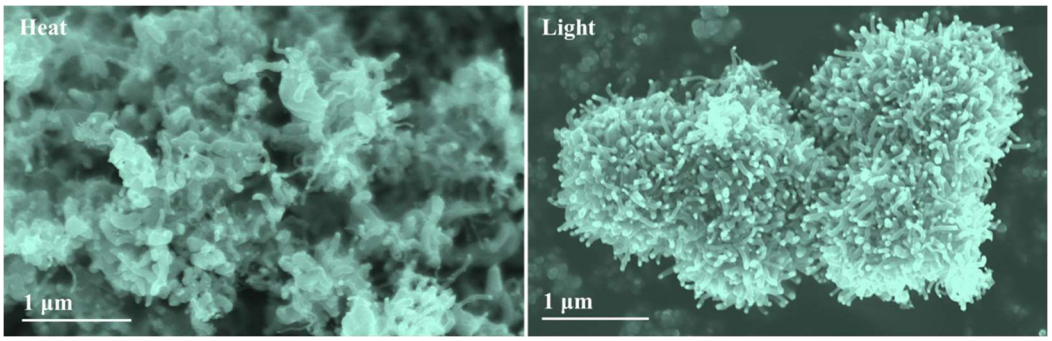

Fig. S19. SEM images of Co_3O_4 after a 10-h thermocatalytic reaction at 400 °C and a 10-h photochemical reaction at ambient temperature.

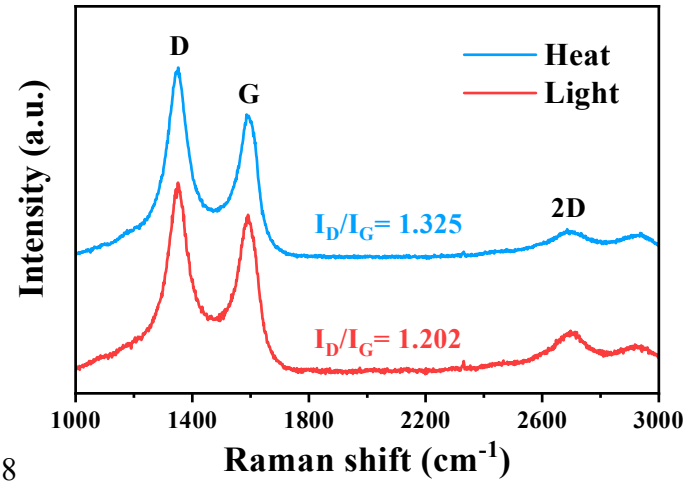

Fig. S20. Raman spectra of Co_3O_4 after a 10-h thermocatalytic reaction at 400 °C and a 10-h photochemical reaction at ambient temperature.

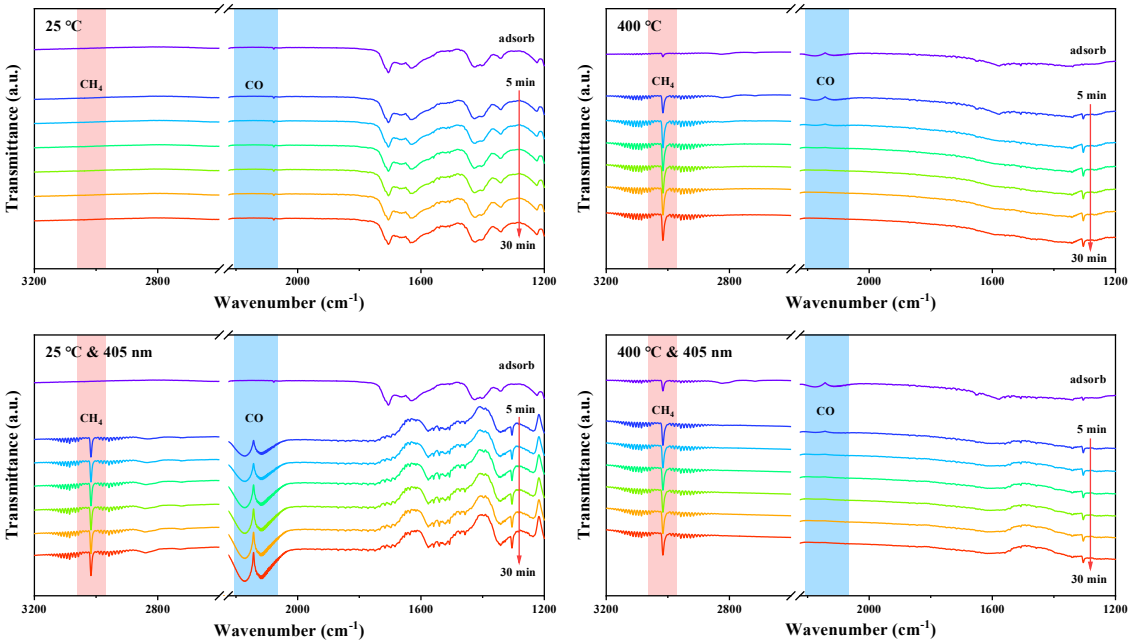

312

313 **Fig. S21.** In-situ DRIFTS of CO_2 hydrogenation on Co_3O_4 catalyst at 25 and 400 °C
314 with and without light illumination from a 405 nm LED.

315

316

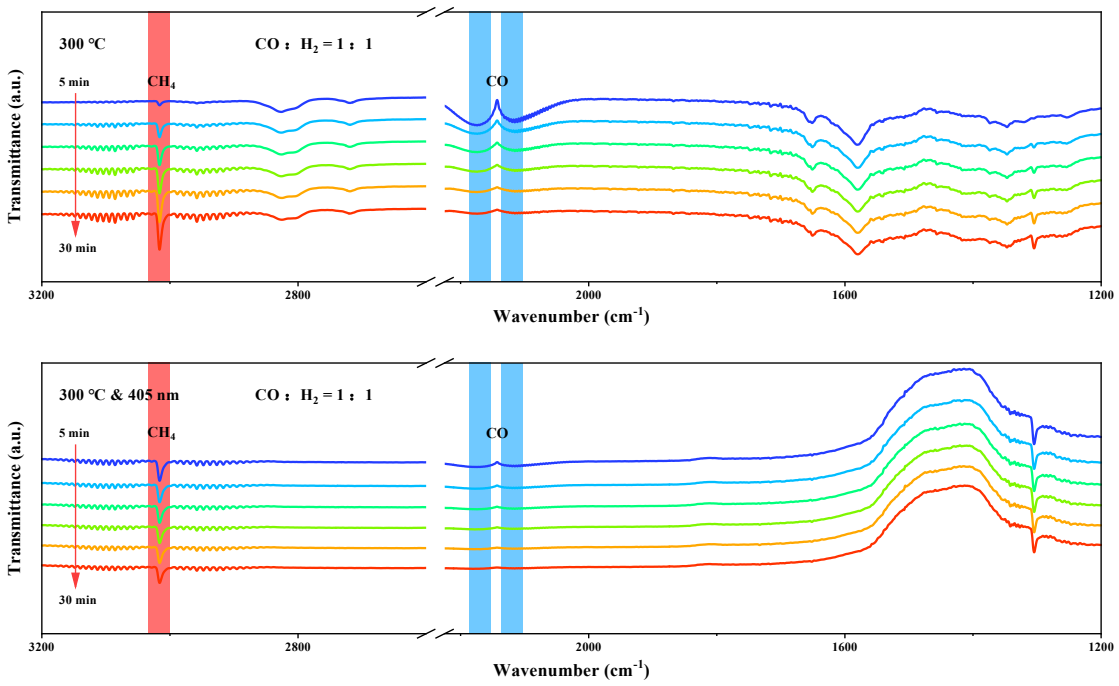

317

318 **Fig. S22.** In-situ DRIFTS of CO hydrogenation on Co_3O_4 catalyst at 300 °C with and
319 without light illumination from a 405 nm LED.

320

321

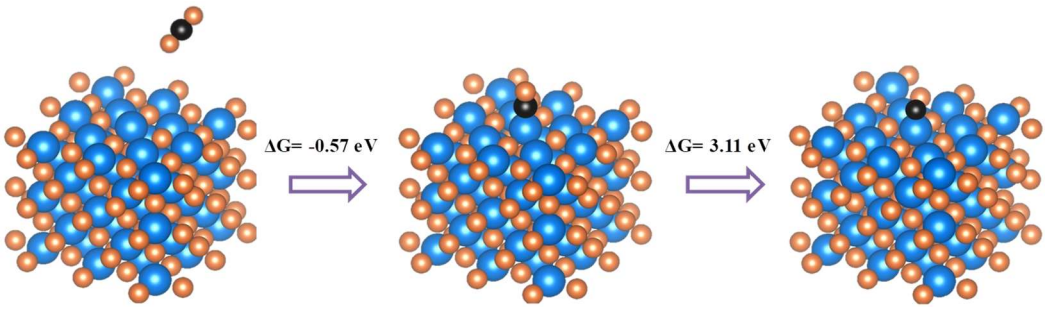

Fig. S23. The potential energy profile of CO_2 hydrogenation on CoO (100).

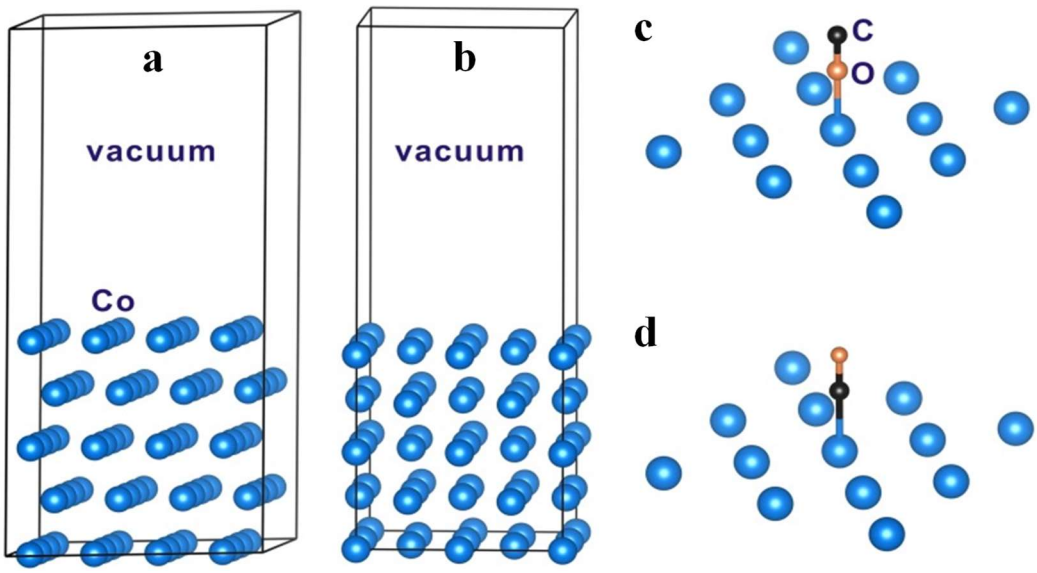

Fig. S24. Slab models of 4 × 4 hcp-Co (001) (**a**) and 2 × 2 fcc-Co (100) (**b**) surfaces. **c** and **d** are two possible initial models of the fcc-Co (100) surfaces with adsorbed CO.

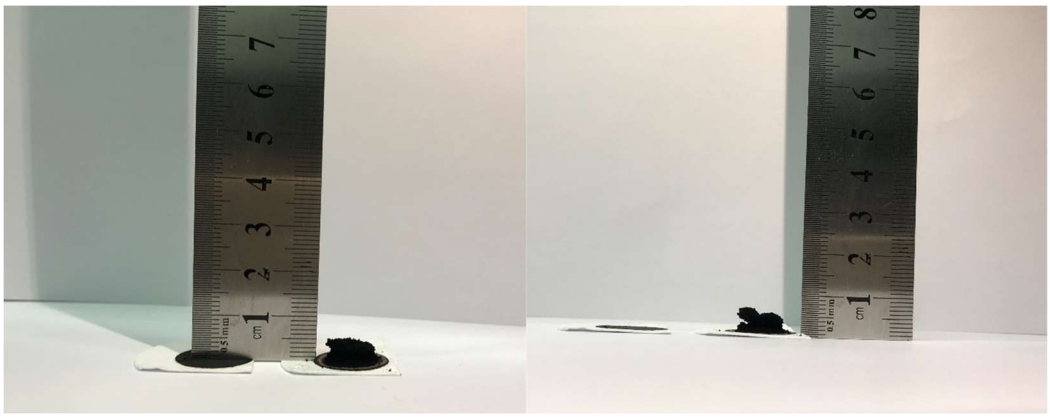

Fig. S25. Photographs of Co_3O_4 catalyst before and after a multi-run (10 h/run) photochemical reaction at 1 MPa.

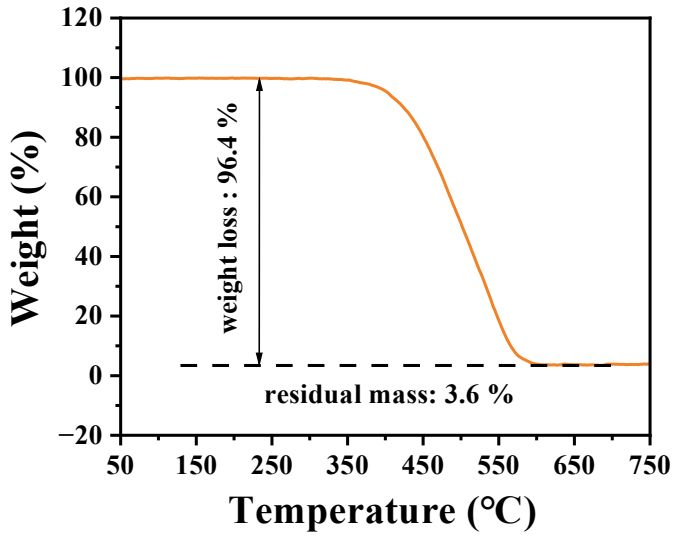

337

338 **Fig. S26.** TG curves of the catalyst (5 mg) after a multi-run (10 h/run) photochemical
339 reaction at 1 MPa.

340

341

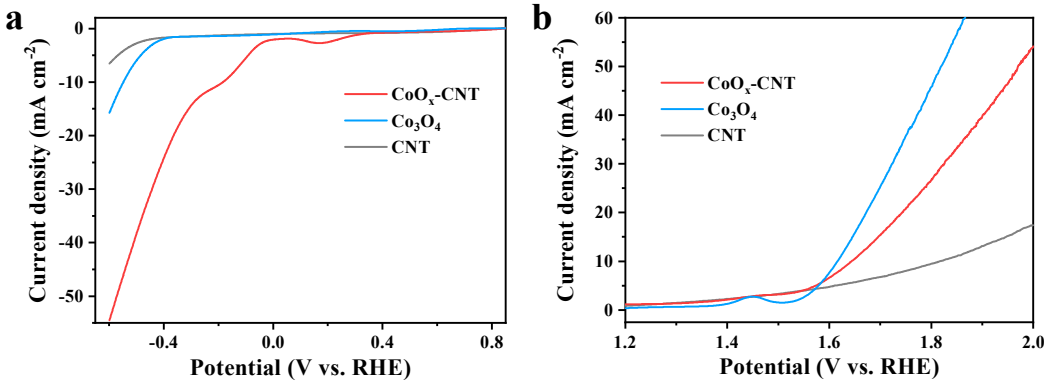

342

343 **Fig. S27.** Linear sweep voltammetry curves of CoO_x-CNT, Co_3O_4 and CNT in 1 M
344 NaOH (pH=13.6) for hydrogen evolution reaction (**a**) and oxygen evolution reaction
345 (**b**).

346

347

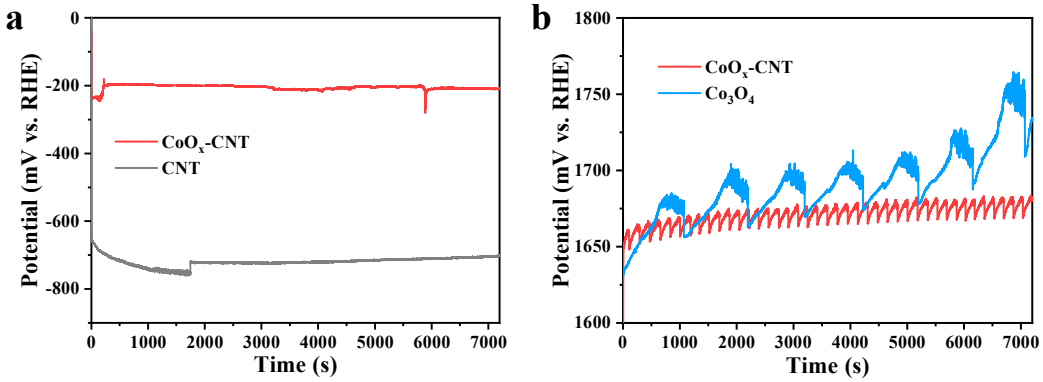

348

349 **Fig. S28.** The chronopotentiometric curves of CoO_x-CNT, Co_3O_4 and CNT at a constant
350 current density for hydrogen evolution reaction (–10 mA cm^{-2}) (**a**) and oxygen
351 evolution reaction (10 mA cm^{-2}) (**b**).

352

353

354 **Table S1.** Curvefit parameters for Co K-edge EXAFS of CoO_x.

355

Path	D[b] / Å	CN	R / Å	σ^2 / Å^2
Co–O	2.132	1.5(3)	2.08(1)	0.006(1)
Co–Co1	2.506	8.6(6)	2.50(1)	0.006(1)[c]
Co–Co2	3.014	3.2(4)	3.00(1)	0.006(1)[c]

356

357 [a] S_0^2 was fixed as 0.75. ΔE_0 was refined as a global fit parameter, returning a value of (−4 ± 1) eV.
358 Data ranges: 2.5 ⩽ k ⩽ 13.8 Å^{-1}, 1.0 ⩽ R ⩽ 2.9 Å. The number of variables is 9, out of a
359 total of 13.4 independent data points. R factor for this fit is 0.5%. [b] The distance for Co–O and Co–
360 Co2 are from the crystal structure of CoO. The distance for Co–Co1 is from the crystal structure of
361 Co. [c] The Debye–Waller factors were constrained as σ^2(Co–Co1) = σ^2(Co–Co2) for decreasing the
362 correlation (or reducing the number of variables).

363

364

Table S2. The calculated free energies (eV) of different slab models.

Slab models	On hcp Co (001) surface	On fcc Co (100) surface
*	−528.75	−256.67
*(CO_2)	−551.73	−279.70
*(HOCO)	−555.06	−282.85
*(CO+OH)	−556.55	−284.55
*(CO)	−545.41	−273.03
*(C+O)	−545.55	−274.83
*(COH)	−547.13	−274.74
*(C+OH)	−548.79	−277.65

The * denotes substrate.

Supplementary References

[1] G. Kresse, J. Hafner, Phys. Rev. B 47, 558 (1993).

[2] P.E. Blöchl, Phys. Rev. B 50, 17953 (1994).

[3] J.P. Perdew, J. Chevary, S. Vosko, K.A. Jackson, M.R. Pederson, D. Singh, C. Fiolhais, Phys. Rev. B 46, 6671 (1992).

[4] J.P. Perdew, K. Burke, M. Ernzerhof, Phys. Rev. Lett. 77, 3865−3868(1996).

[5] G. Jones, J.G. Jakobsen, S.S. Shim, J. Kleis, M.P. Andersson, J. Rossmeisl, F. Abild-Pedersen, T. Bligaard, S. Helveg, B. Hinnemann, J.R. Rostrup-Nielsen, I. Chorkendorff, J. Sehested, J.K. Nørskov, J. Catal. 259, 147−160(2008).

[6] V. Wang, N. Xu, J.-C. Liu, G. Tang, W.-T. Geng, Comput. Phys. Commun. 267, 108033(2021).

[7] A. Nakhaei Pour, Z. Keyvanloo, M. Izadyar, S.M. Modaresi, Int. J. Hydrogen Energy 40, 7064−7071(2015).

[8] P. van Helden, I.M. Ciobîcă, ChemPhysChem 12, 2925−2928(2011).